Metadata of the chapter that will be visualized in SpringerLink

Book Title	Machine Learning in Medical Imaging	
Series Title		
Chapter Title	Segmentation-Free Estimation of Kidney Volumes in CT with Dual Regression Forests	
Copyright Year	2016	
Copyright HolderName	Springer International Publishing AG	
Corresponding Author	Family Name	**Hussain**
	Particle	
	Given Name	**Mohammad Arafat**
	Prefix	
	Suffix	
	Division	Department of Electrical and Computer Engineering
	Organization	University of British Columbia
	Address	Vancouver, BC, Canada
	Email	arafat@ece.ubc.ca
Author	Family Name	**Hamarneh**
	Particle	
	Given Name	**Ghassan**
	Prefix	
	Suffix	
	Division	School of Computing Science
	Organization	Simon Fraser University
	Address	Burnaby, BC, Canada
	Email	hamarneh@sfu.ca
Author	Family Name	**O'Connell**
	Particle	
	Given Name	**Timothy W.**
	Prefix	
	Suffix	
	Division	Division of Emergency and Trauma Radiology
	Organization	Vancouver General Hospital
	Address	Vancouver, BC, Canada
	Email	tim.oconnell@gmail.com
Author	Family Name	**Mohammed**
	Particle	
	Given Name	**Mohammed F.**
	Prefix	
	Suffix	
	Division	Division of Emergency and Trauma Radiology
	Organization	Vancouver General Hospital
	Address	Vancouver, BC, Canada

	Email	mohammed.f.mohammed@gmail.com
Author	Family Name	**Abugharbieh**
	Particle	
	Given Name	**Rafeef**
	Prefix	
	Suffix	
	Division	Department of Electrical and Computer Engineering
	Organization	University of British Columbia
	Address	Vancouver, BC, Canada
	Email	rafeef@ece.ubc.ca

Abstract

Accurate estimation of kidney volume is essential for clinical diagnoses and therapeutic decisions related to renal diseases. Existing kidney volume estimation methods rely on an intermediate segmentation step that is subject to various limitations. In this work, we propose a segmentation-free, supervised learning approach that addresses the challenges of accurate kidney volume estimation caused by extensive variations in kidney shape, size and orientation across subjects. We develop dual regression forests to simultaneously predict the kidney area per image slice, and kidney span per image volume. We validate our method on a dataset of 45 subjects with a total of 90 kidney samples. We obtained a volume estimation accuracy higher than existing segmentation-free (by 72 %) and segmentation-based methods (by 82 %). Compared to a single regression model, the dual regression reduced the false positive area-estimates and improved volume estimation accuracy by 41 %. We also found a mean deviation of under 10 % between our estimated kidney volumes and those obtained manually by expert radiologists.

Segmentation-Free Estimation of Kidney Volumes in CT with Dual Regression Forests

Mohammad Arafat Hussain[1(✉)], Ghassan Hamarneh[2], Timothy W. O'Connell[3], Mohammed F. Mohammed[3], and Rafeef Abugharbieh[1]

[1] Department of Electrical and Computer Engineering, University of British Columbia, Vancouver, BC, Canada
{arafat,rafeef}@ece.ubc.ca
[2] School of Computing Science, Simon Fraser University, Burnaby, BC, Canada
hamarneh@sfu.ca
[3] Division of Emergency and Trauma Radiology, Vancouver General Hospital, Vancouver, BC, Canada
tim.oconnell@gmail.com, mohammed.f.mohammed@gmail.com

Abstract. Accurate estimation of kidney volume is essential for clinical diagnoses and therapeutic decisions related to renal diseases. Existing kidney volume estimation methods rely on an intermediate segmentation step that is subject to various limitations. In this work, we propose a segmentation-free, supervised learning approach that addresses the challenges of accurate kidney volume estimation caused by extensive variations in kidney shape, size and orientation across subjects. We develop dual regression forests to simultaneously predict the kidney area per image slice, and kidney span per image volume. We validate our method on a dataset of 45 subjects with a total of 90 kidney samples. We obtained a volume estimation accuracy higher than existing segmentation-free (by 72 %) and segmentation-based methods (by 82 %). Compared to a single regression model, the dual regression reduced the false positive area-estimates and improved volume estimation accuracy by 41 %. We also found a mean deviation of under 10 % between our estimated kidney volumes and those obtained manually by expert radiologists.

AQ1

1 Introduction

The economic burden of chronic kidney disease (CKD) is significant, estimated in Canada in 2007 at $1.9 Billion just for patients with end-stage renal disease (ESRD) [1]. In 2011, about 620,000 patients in United States received treatment for ESRD either by receiving dialysis or by receiving kidney transplantation [2]. ESRD is the final stage of different CKDs, e.g. Autosomal dominant polycystic kidney disease (ADPKD), renal artery atherosclerosis (RAS), which are associated with the change of kidney volume. However, detection of CKDs are complicated; multiple tests such as the estimated glomerular filtration rate (eGFR) and serum albumin-to-creatinine ratio may not detect early disease and may be poor

L. Wang et al. (Eds.): MLMI 2016, LNCS 10019, pp. 1–8, 2016.
DOI: 10.1007/978-3-319-47157-0_19

at tracking progression of disease [3]. Recent works [2,4] have suggested kidney volume as the potential surrogate marker for renal function and is thus useful for predicting and tracking the progression of different CKDs. In fact, the *total kidney volume* has become the gold-standard image biomarker for the ADPKD and RAS progression at early stages of this disease [4]. In addition, the renal volumetry has recently emerged as the most suitable alternative to renal scintigraphy in evaluating the *split renal function* in kidney donors as well as the best biomarker in follow-up evaluation of kidney transplants [2]. Consequently, estimation of the 'volume' of a kidney has become the primary objective in various clinical analyses of kidney.

Traditionally, the kidney volume is estimated by means of segmentation. However, existing kidney segmentation algorithms have various limitations (e.g. requiring user interaction, sensitivity to parameter setting, heavy computation). For example, Yan et al. [5] proposed a simple intensity thresholding-based method, which is often inaccurate and was limited to 2D. Other intensity-based methods have used graph cuts [6] and active contours/level sets [7]. But these methods are sensitive to the choice of parameters [8], which often need to be tweaked for different images. In addition, the graph cuts [6] and level sets-based [7] methods are prone to leaking through weak anatomical boundaries in the image, and often require considerable computation [8]. The method proposed by Lin et al. [9] relies extensively on prior knowledge of kidney shapes. However, building a realistic model of kidney shape variability and balancing the influence of the model on the resulting segmentation are non-trivial tasks.

To overcome the aforementioned limitations of the traditional methods, a number of kidney segmentation methods have been proposed based on supervised learning [10–12]. Cuingnet et al. [10] used a classification forest to generate a kidney spatial probability map and then deformed a ellipsoidal template to approximate the probability map and generate the segmentations. Due to this restrictive template-based approach, it is likely to fail for kidneys having abnormal shape due to disease progression and/or internal tumors. Therefore, crucially, [10] did not include the truncated kidneys (16 % of their data) in their evaluation. Even then, their proposed method did not correctly detect/segment about 20 % of left and 20 % of right, and failed for another 10 % left and 10 % right kidneys of their evaluation data set. Glocker et al. [11] used a joint classification-regression forest scheme to segment different abdominal organs, but their approach suffers from leaking, especially for kidneys, as evident in their results. Thong et al. [12] showed promising kidney segmentation performance using convolutional networks, however, it was designed only for 2D contrast-enhanced computed tomography (CT) slices.

Recently, supervised learning-based direct volume estimation methods, which eliminate the segmentation step altogether, have become attractive and shown promise in cardiac bi-ventricular volumetry [8,13]. These methods can effectively bypass the computation complexities and limitations of segmentation-based approaches while producing accurate volume estimates. Although these methods require manual segmentation during the training phase; once deployed,

the trained algorithm can respond to quick clinical queries by skipping the segmentation step. This idea of direct volume estimation can be effectively adapted to kidneys, when inferring the scalar-valued kidney volume (e.g. in mm^3) is the ultimate goal. But kidney anatomy varies more extensively across patients than that of the target anatomy in [8,13]. Therefore, a more robust learning-based direct approach is necessary for accurate estimation of kidney volumes.

In this paper, we propose a novel method for direct estimation of kidney volumes for 3D CT images with dual regression forests that omits the error-prone segmentation step. Given an approximate kidney location within the 3D CT images, our method uses dual random forests, one to predict the kidney area in each axial image plane, and another to enhance the results by removing outliers from the initially estimated areas. We adopt a smaller subpatch-based approach instead of a full 2D patch (as in [8,13]) in order to increase the number of observations, which ultimately improved our results. Using this novel combination of 'dual regression' and 'subpatch', our method outperforms the single forest+full patch-based method [13]. We use kidney appearance, namely intensity and texture information to generate features. Note that kidney localization (i.e. locating a 3D kidney bounding box inside the full CT volume) is not the aim of our work since quick manual localization is acceptable for the clinical workflow, as confirmed by our clinical collaborators. Nevertheless, existing localization methods may be applied prior to using our method, e.g. [10]. Even if only a crude auto-localization is available, our method performs inference on a generously bigger bounding box to avoid any kidney truncation.

2 Methods

Our volume estimation technique is divided into three steps as shown in Fig. 1. In Sect. 2.1, we discuss the 2D image patch representation. Then, in Sect. 2.2, we discuss the training of regression forests and subsequent prediction of kidney areas. Finally, in Sect. 2.3, we discuss the estimation of kidney volumes based on predictions by the dual regression forests.

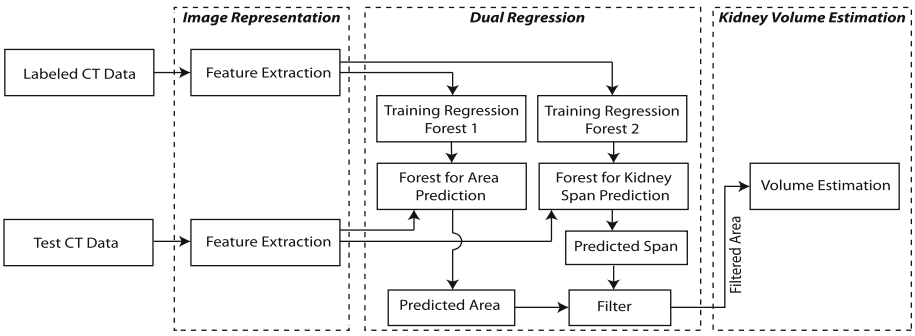

Fig. 1. Flowchart showing different components of the proposed method.

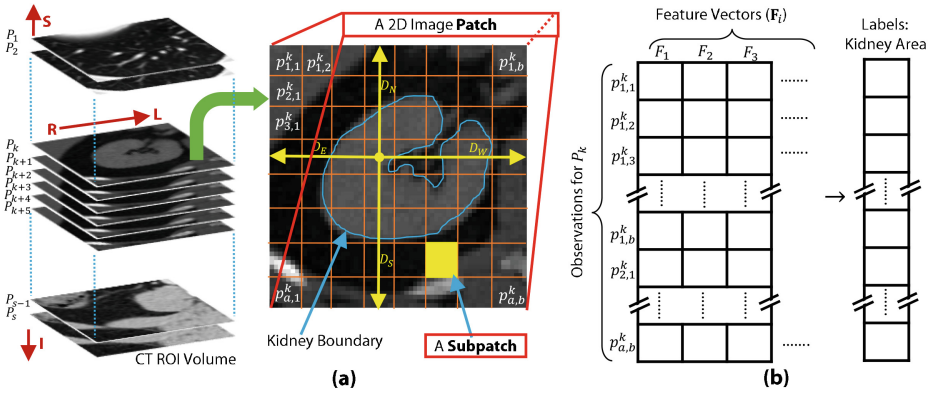

Fig. 2. Illustration of (a) the representation of our 2D image patch containing kidney, and (b) the formation of feature vectors from its subpatches.

2.1 Image Representation

We divide each image patch into square subpatches (Fig. 2(a)). Then, in order to obtain the prediction of the kidney area for each of the sub-patches, we train a regression forest with these sub-patches as observations. We use various features $\mathbf{F}_i$ for each subpatch p: (1) the sum of image intensities $\sum_p I$; (2) sum of non-overlapped binned intensities $\sum_p I_b$, where b stands for different bin numbers and $\min(I) \leq I_b \leq \max(I)$; (3) entropy $E = -\sum h \times log_2(h)$, where h are the histogram counts of I; (4) sum of image intensity ranges $\sum_p R$, which is (max value - min value) in a 3×3 pixel neighborhood around the corresponding pixel; (5) sum of standard deviations $\sum_p SD$, where SD is estimated in a 3×3 neighborhood pixels around the corresponding pixel; and (6) axially aligned distances D_E, D_W, D_N and D_S of the interrogated subpatch center from the east, west, north and south boundaries of the 2D image patch, respectively (Fig. 2(a)). Features (3)–(5) capture the texture information in each subpatch.

2.2 Learning and Prediction

Regression forest 1 (Fig. 1) learns the correspondence between input features and kidney areas for training subpatches, and then predicts kidney areas in unseen subpatches. For feature matrix $v = (\mathbf{F}_1, \mathbf{F}_2, ..., \mathbf{F}_d)$, where $\mathbf{F}_i$ is a feature vector (Fig. 2(b)) and d is the total number of features, forest 1 learns to associate observations $\mathbf{F}_i(r, s)$, $(i = 1, .., d)$ with a continuous scalar value $y^k(r, s)$ which is the estimated kidney area in the corresponding subpatch $p^k_{r,s}$. Here, k is the patch index, and r and s are the subpatch indices along the posterior-anterior (P-A) and right-left (R-L) directions, respectively. The distribution of estimated kidney area values $D(\tilde{y})$ *vs.* subpatches for a kidney sample is shown in Fig. 3(b). However, due to extensive variation in kidney shapes, sizes and orientations across subjects, we observed that non-zero volumes are predicted for areas devoid of

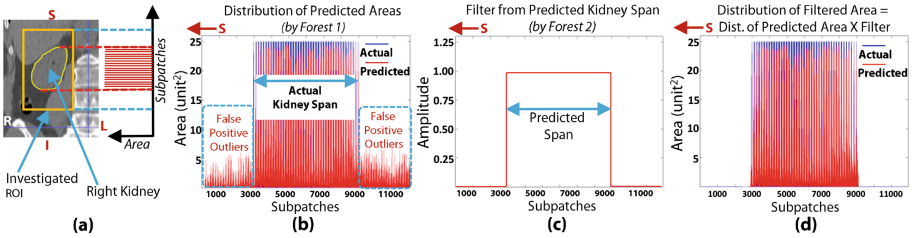

Fig. 3. (a) Schematic diagram showing an example investigated ROI and its most likely kidney-area *vs.* subpatches distribution. (b) A typical distribution of predicted kidney-area *vs.* subpatches (red), overlaid on the actual kidney-area *vs.* subpatches (deep blue). Predicted areas include false positive outliers as shown with the light-blue dashed-boxes. (c) An example plot of a predicted kidney span. (d) The final distribution of the filtered kidney-area *vs.* subpatches, overlaid on the actual kidney-area *vs.* subpatches where most of the outliers are removed. (Color figure online)

kidney tissue (Figs. 3(a) and (b)). These false positives are removed using a spatial filter (Fig. 3(c)) having an extent (or bandwidth) equal to a spatial kidney span measure (along superior-inferior direction). This important span parameter is learnt by forest 2. For training forest 2, we rearrange (i.e. negligible extra computations) the feature vectors as $\hat{\mathbf{F}}_i^k = \sum_{m=1}^{a\times b} \mathbf{F}_i^k(m)$, where a and b are the total number of subpatches along the P-A and R-L directions, respectively. We define a unit step function $U(\tilde{u})$ whose spatial bandwidth is equivalent to the span $\tilde{u}$ predicted by forest 2 for a particular kidney sample (Fig. 3(c)). We approximate the most probable kidney span in the false positives-corrupted D by calculating the cross-correlation between D and U defined as $\rho(l) = \sum_{q=1}^{Q} D(q) \cdot U(q+l)$, where Q is the total number of subpatches in an investigated ROI containing kidney. The lag corresponding to the maximum of $\rho(l)$, $l_{max} = \text{argmax}_l\{\rho(l)\}$ is then used to align U with D. Finally, an element-wise multiplication $D \cdot U$ generates the filtered area distribution (D_f), where almost all of the false positives are removed (Fig. 3(d)). Note that although we use subpatches, we are not labeling every pixel, as done for classification-based segmentation in [10–12], but rather inferring a scalar area for every subpatch.

2.3 Kidney Volume Estimation

There are some subpatches that completely lie inside the kidney cross-section, and we expect the predicted kidney areas for those subpatches to be the maximum, S_A (area of a subpatch). However, we observed that almost no predicted-subpatch-area (by forest 1) reaches this obvious maximum value S_A. On the other hand, there are few false positives still left inside the filtered area distribution D_f. We therefore choose an empirical threshold g and fine tune D_f as: $D_f(p) = 0$, if $D_f(p) < g$, and $D_f(p) = S_A$, if $S_A - D_f(p) < g$. Finally, we estimate the volume of a kidney by integrating the areas in D_f in the axial direction.

3 Validation Setup

We acquired abdominal CT images from 45 patients using the CT scanner Siemens SOMATOM Definition Flash (Siemens Healthcare GmbH, Erlangen, Germany) at Vancouver General Hospital, Vancouver, BC, Canada with all ethics review board approvals in place. Prior to image acquisition, 30 of the patients were injected with a contrast agent. We were able to use a total of 90 kidney samples (both left and right kidneys) from which 46 samples (from 23 randomly chosen patients) were used for training and the rest as unseen. The in-plane pixel size ranged from 0.67 to 0.98 mm and the slice thickness ranged from 1.5 to 3 mm. The ground truth kidney volumes (referred to as 'actual volumes') were calculated from kidney delineations performed by expert radiologists. We used a leave-one-kidney-sample-out cross-validation approach on the training set to choose suitable tree and leaf sizes. We use the subpatch size 5×5 pixels, and $g = S_A/5$ throughout the paper.

4 Results

We provide comparative results of our proposed method with those obtained by four generic approaches: two segmentation algorithms, a naïve clinical method, a deep learning method, and three forest-based approaches. But first, we show the performance of the proposed method visually in Fig. 4(a) where we illustrate the correlation between the actual and estimated kidney volumes. This figure shows that, aside from few exceptions, almost all of the estimates are close to their corresponding ground truth measurements.

We also show the performance comparison of the execution time, volume estimation accuracy, and extra-time requirements for parameter optimization for different methods in Fig. 4(b). We see in Fig. 4(b): rows 1 & 2 that it was necessary to use extra-time for kidney-sample-wise parameter optimization for both

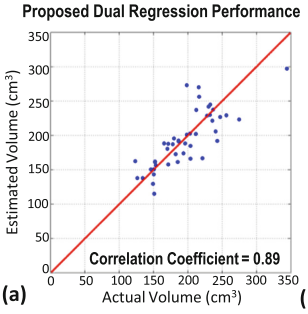

(a) (b)

Row	Generic Methods		Method Tools	Execution Time *per* Run *per* Sample (seconds)	Extra-time for Parameter Optimization	Mean Volume Error (%)
1	Segmentation		Intensity Thresholding	1.10 ± 0.06	Moderate	67.57 ± 114.10
2	Segmentation		3D Active Contour [7]	70.10 ± 10.19	Extensive	55.91 ± 98.17
3	Naïve Clinical Approach		Manual Ellipsoid Fitting	~180	None	14.20 ± 13.56
4	*Segmentation Free*	Deep Learning	Convolutional Neural Network (CNN) + **2D Patches**	0.15 ± 0.0089 §	None	16.42 ± 13.56
5	*Segmentation Free*	Regression Forests	Single Regression + **2D Patches** [13]	1.57 ± 0.09	None	36.14 ± 20.86
6	*Segmentation Free*	Regression Forests	Single Regression + **2D Subpatches**	1.88 ± 0.12	None	16.88 ± 10.82
7	*Segmentation Free*	Regression Forests	Single Regression + **3D Subpatches**	1.02 ± 0.04	None	26.88 ± 20.11
8	*Segmentation Free*	Regression Forests	**Proposed Dual Regression**	3.75 ± 0.23	None	9.97 ± 8.69

§ With Nvidia GeForce GTX 460 v2 GPU with 1GB of GDDR5 VRAM

Fig. 4. (a) Scatter plot showing the volume correlations between the actual and proposed dual regression-based estimates, and (b) a table showing a comparison of volume estimation accuracies, estimation speeds, and requirements of extra-time for parameter optimization during the execution for different types of methods. Execution time is the Matlab(R) runtime on Intel(R) Xeon(R) CPU E3 @ 3.20GHz with 8 GB RAM.

segmentation-based approaches. Although it is possible to find optimal settings of parameters for active contours and other energy-minimizing segmentation methods through cross-validation, the pursuit for optimal parameters is computationally expensive and near infeasible. We also see in row 1 that the estimated mean volume error (MVE) for the intensity thresholding-based method is the highest since it cannot differentiate between two different organs if the intensities associated with these organs fall inside the same user-defined/automatically chosen range. On the other hand, the 3D active contours-based method [7] produces kidney surface which leaks through the weaker boundaries even with the most optimal empirical parameter configuration. As a result, the MVE performance is poor (Fig. 4(b): row 2). Moreover, it is time inefficient as well.

Then we consider a manual approach which is typically used by the radiologists in the clinical settings. The experts obtain three major axes on a kidney, which correspond to a 3D ellipsoid that approximates that particular kidney. In Fig. 4(b): row 3, we see that the estimated MVE (computed by expert radiologists) for this approach is approximately 15 % with high standard deviations. In addition, it takes around 3 min per kidney sample.

Next we consider a segmentation-free convolutional neural network-based deep learning method, where a particular 2D image patch (see Fig. 2(a)) is used as a single observation domain. We see in Fig. 4(b): row 4, that the estimated MVE is similar to that of single forest+2D subpatch-based approach (row 6) but is worse, however, than the manual clinical approach (row 3).

Finally, we consider four segmentation-free approaches using regression forests. The first approach [13] uses single forest+2D patch and the corresponding MVE performance is poor as seen in row 5. This approach works well for cardiac bi-ventricles but fails for kidney, since sizes, shapes and orientations of kidneys vary more extensively across subjects. Subsequently, we adopt an efficient approach of learning using image subpatches (5×5 pixels). This subpatch-based approach improves the MVE performance than that of the patch-based approach (see rows 5 & 6). However, these subpatch-based results are still corrupted by the false positive estimates. We also tested using 3D subpatches ($5 \times 5 \times 2$ voxels). Since CT axial resolution is lower than those of the coronal and sagittal, $5 \times 5 \times 2$ closely resembles a cube shape. However, we see in row 7 that the corresponding MVE is worse than that of 2D subpatches (row 6). We suspect that this poor performance may be caused by the reduced number of training samples. The proposed method (dual regression+2D subpatch) combines the 2D subpatch-based area prediction and patch-based kidney span prediction, which ultimately gives the best improvement of volume estimation. While the mean accuracy of the forest 2-based kidney span prediction is approximately 95.5 % alone, the Table (row 8) shows that the MVE by the proposed method falls below 10 %, with the cost of a prediction time of $\sim$4 sec per kidney sample, which can be further accelerated via a GPU-implementation.

5 Conclusions

In this paper, we proposed an effective method for direct estimation of kidney volumes from 3D CT images. We formulated our volume estimation problem

as a 2D subpatch learning-based regression problem and were able to avoid the problematic segmentation step. Though kidney shapes, sizes and orientations vary extensively across subjects, we addressed this challenge by adopting a dual regression forest formulation that were trained by making use of the same extracted image features and their combined predictions resulted in satisfactory kidney volume estimates. Our experimental results showed that the proposed method can estimate kidney volumes with high correlation compared with those obtained manually by expert radiologists (89 %) and reported the MVE of 10 %.

References

1. Zelmer, J.L.: The economic burden of end-stage renal disease in canada. Kidney Int. Masson SAS. **72**(9), 1122–1129 (2007)
2. Diez, A., Powelson, J., et al.: Correlation between CT-based measured renal volumes and nuclear-renography-based SRF in living kidney donors. clinical diagnostic utility and practice patterns. Clin. Transplant. **28**(6), 675–682 (2014)
3. Connolly, J.O., Woolfson, R.G.: A critique of clinical guidelines for detection of individuals with chronic kidney disease. Neph. Clin. Pract. **111**(1), c69–c73 (2009)
4. Widjaja, E., Oxtoby, J.W., et al.: Ultrasound measured renal length vs. low dose CT volume in predicting single kidney GFR. Br. J. Radiol. **77**, 759–764 (2014)
5. Yan, G., Wang, B.: An automatic kidney segmentation from abdominal CT images. IEEE Intell. Comput. Intell. Syst. **1**, 280–284 (2010)
6. Li, X., Chen, X., Yao, J., Zhang, X., Tian, J.: Renal cortex segmentation using optimal surface search with novel graph construction. In: Fichtinger, G., Martel, A., Peters, T. (eds.) MICCAI 2011. LNCS, vol. 6893, pp. 387–394. Springer, Heidelberg (2011). doi:10.1007/978-3-642-23626-6_48
7. Zhang, Y., Matuszewski, B.J., Shark, L.K., Moore, C.J.: Medical image segmentation using new hybrid level-set method. In: BioMedical Visualization, pp. 71–76 (2008)
8. Zhen, X., Wang, Z., Islam, A., Bhaduri, M., Chan, I., Li, S.: Multi-scale deep networks and regression forests for direct bi-ventricular volume estimation. Med. Image Anal. **30**, 120–129 (2016)
9. Lin, D.T., Lei, C.C., Hung, S.W.: Computer-aided kidney segmentation on abdominal CT images. IEEE Trans. Inf. Tech. Biomed. **10**(1), 59–65 (2006)
10. Cuingnet, R., Prevost, R., Lesage, D., Cohen, L.D., Mory, B., Ardon, R.: Automatic detection and segmentation of kidneys in 3D CT images using random forests. In: Ayache, N., Delingette, H., Golland, P., Mori, K. (eds.) MICCAI 2012. LNCS, vol. 7512, pp. 66–74. Springer, Heidelberg (2012). doi:10.1007/978-3-642-33454-2_9
11. Glocker, B., Pauly, O., Konukoglu, E., Criminisi, A.: Joint classification-regression forests for spatially structured multi-object segmentation. In: European Conference on Computer Vision, pp. 870–881 (2012)
12. Thong, W., Kadoury, S., Piche, N., Pal, C.J.: Convolutional networks for kidney segmentation in contrast-enhanced CT scans. Comput. Methods Biomech. Biomed. Eng.: Imaging Visual., 1–6 (2016)
13. Zhen, X., Wang, Z., Islam, A., Bhaduri, M., Chan, I., Li, S.: Direct estimation of cardiac bi-ventricular volumes with regression forests. In: Golland, P., Hata, N., Barillot, C., Hornegger, J., Howe, R. (eds.) MICCAI 2014. LNCS, vol. 8674, pp. 586–593. Springer, Heidelberg (2014). doi:10.1007/978-3-319-10470-6_73

Author Queries

Chapter 19

Query Refs.	Details Required	Author's response
AQ1	Please confirm if the corresponding author is correctly identified. Amend if necessary.	

MARKED PROOF

Please correct and return this set

Please use the proof correction marks shown below for all alterations and corrections. If you wish to return your proof by fax you should ensure that all amendments are written clearly in dark ink and are made well within the page margins.

Instruction to printer	*Textual mark*	*Marginal mark*
Leave unchanged	··· under matter to remain	
Insert in text the matter indicated in the margin		New matter followed by or
Delete	through single character, rule or underline or through all characters to be deleted	or
Substitute character or substitute part of one or more word(s)	through letter or through characters	new character or new characters
Change to italics	under matter to be changed	
Change to capitals	under matter to be changed	
Change to small capitals	under matter to be changed	
Change to bold type	under matter to be changed	
Change to bold italic	under matter to be changed	
Change to lower case	Encircle matter to be changed	
Change italic to upright type	(As above)	
Change bold to non-bold type	(As above)	
Insert 'superior' character	through character or where required	or under character e.g. or
Insert 'inferior' character	(As above)	over character e.g.
Insert full stop	(As above)	
Insert comma	(As above)	
Insert single quotation marks	(As above)	or and/or or
Insert double quotation marks	(As above)	or and/or or
Insert hyphen	(As above)	
Start new paragraph		
No new paragraph		
Transpose		
Close up	linking characters	
Insert or substitute space between characters or words	through character or where required	
Reduce space between characters or words	between characters or words affected	